Article

Tunnelling measured in a very slow ion–molecule reaction

https://doi.org/10.1038/s41586-023-05727-z

Received: 13 July 2022

Accepted: 12 January 2023

Published online: 1 March 2023

Check for updates

Robert Wild[1], Markus Nötzold[1], Malcolm Simpson[1], Thuy Dung Tran[1,2] & Roland Wester[1]✉

Quantum tunnelling reactions play an important role in chemistry when classical pathways are energetically forbidden[1], be it in gas-phase reactions, surface diffusion or liquid-phase chemistry. In general, such tunnelling reactions are challenging to calculate theoretically, given the high dimensionality of the quantum dynamics, and also very difficult to identify experimentally[2–4]. Hydrogenic systems, however, allow for accurate first-principles calculations. In this way the rate of the gas-phase proton-transfer tunnelling reaction of hydrogen molecules with deuterium anions, $H_2 + D^- \rightarrow H^- + HD$, has been calculated[5], but has so far lacked experimental verification. Here we present high-sensitivity measurements of the reaction rate carried out in a cryogenic 22-pole ion trap. We observe an extremely low rate constant of $(5.2 \pm 1.6) \times 10^{-20}$ cm^3 s^{-1}. This measured value agrees with quantum tunnelling calculations, serving as a benchmark for molecular theory and advancing the understanding of fundamental collision processes. A deviation of the reaction rate from linear scaling, which is observed at high H_2 densities, can be traced back to previously unobserved heating dynamics in radiofrequency ion traps.

Hydrogen is the most abundant element in the universe[6], and collisions of hydrogen and its charged forms are important in the chemistry and evolution of the interstellar medium[7,8]. Binary collisions of atomic with molecular hydrogen belong to the most fundamental molecular systems to be studied experimentally and are simple enough to be investigated using full quantum calculations[9,10]. Here we investigate the presumably most fundamental ion–molecule reaction: the proton-transfer reaction from hydrogen molecules to hydrogen atomic anions. This reaction, which can be made exoergic by virtue of vibrational zero-point energy differences when working with deuterium anions, may proceed by means of tunnelling through its intermediate barrier (Fig. 1a):

$$D^- + H_2 \rightarrow H^- + HD. \quad (1)$$

The collision complex has the make-up of the H_3^- anion. Its stability and linear structure were proposed[11] in 1937, but later questioned because of the difficulty of accurately calculating the vibrational zero-point energy. Following the calculation of the first three-dimensional potential energy surface, its stability could be theoretically confirmed[12] and later verified experimentally[13]. Interstellar H_3^- could function as a tracer for H^-, which is thought to be abundantly present in the interstellar medium but not yet observed, mainly because it has only one bound electronic state[14].

Experimental investigations of reaction (1) at energies of a few electronvolts and below started in the 1990s. Crossed-beam experiments revealed state-specific cross-sections and angular distributions for an isotopic variant of reaction (1)[15]. These were compared with pioneering quantum scattering calculations[16]. In a guided ion beam experiment, the barrier height of reaction (1) was found to be about 330 meV (ref. [17]). Numerous further theoretical investigations followed, most of which considered energies above the potential barrier (see, for example, refs. [18–20]). For temperatures in the range of a few Kelvin, colliding reactants generally cannot overcome this barrier, but will chiefly react by means of tunnelling, the probability of which typically increases with lower temperatures because of greater lifetimes of intermediate ion–molecule complexes[21]. In ion–molecule collisions, only two tunnelling reactions have been discovered so far[22,23], $NH_3^+ + H_2$ and c-$C_3H_2^+ + H_2$. A semiclassical estimate of the tunnelling probability of reaction (1) indicated a rate coefficient[24] of about 10^{-19} cm^3 s^{-1}. In a previous measurement only an upper bound could be provided[24]. This result prompted ab initio quantum calculations of the reaction probability at low collision energies, and predicted a rate constant two orders of magnitude lower than the experimental upper limits[5].

Here we present a measurement of the low-temperature reaction rate constant of equation (1), providing a benchmark for molecular quantum tunnelling theory. The principle of this measurement is straightforward: negatively charged deuterium ions are loaded into a 22-pole linear radiofrequency (RF) trap, mounted on a closed-cycle helium cryostat[25]. The 22-pole configuration provides a large field-free region to minimize RF heating, as sketched in Fig. 1a (refs. [26,27]). The D^- ions are collisionally cooled with a buffer gas of hydrogen at 10 K, which leads to an estimated collision temperature of 15 ± 5 K due to RF heating (Methods). Once the ions are cooled, more hydrogen gas is added to the trap and maintained at constant density. After a chosen interaction time, the ions are ejected from the trap and mass-selectively measured by means of time-of-flight (ToF) mass spectrometry.

To measure typical ion–molecule reaction rate coefficients, which have magnitudes around 10^{-9} cm^3 s^{-1}, neutral densities of the order of $(10^{10}–10^{12})$ cm^{-3} are commonly used. This implies that trapping times

[1]Institut für Ionenphysik und Angewandte Physik, Universität Innsbruck, Innsbruck, Austria. [2]Present address: Department of Optics, Palacký University, Olomouc, Czech Republic.
✉e-mail: roland.wester@uibk.ac.at

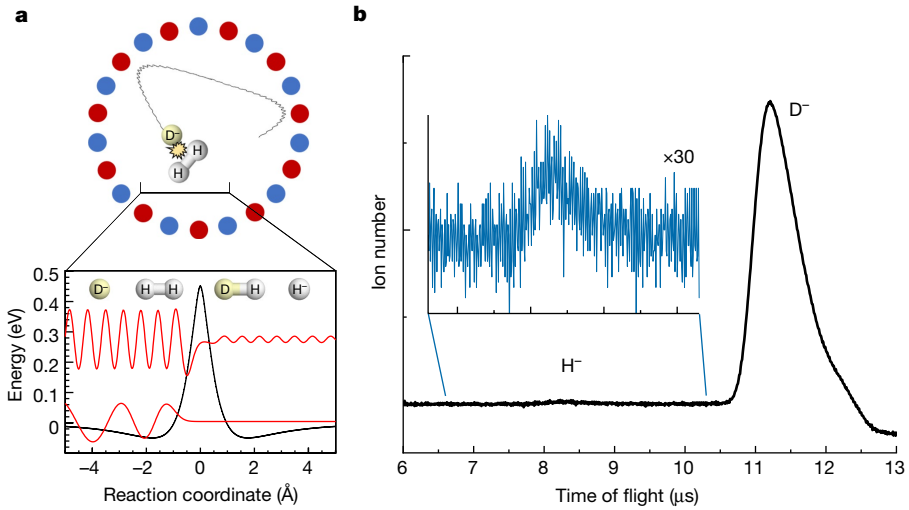

Fig. 1 | Overview of the experiment. a, Cross section of the 22-pole ion trap, viewed along the symmetry axis. An RF voltage is alternately applied to the trap rods (red and blue), trapping D^- ions. During collisions with H_2, proton exchange may occur by means of tunnelling through the reaction barrier, as indicated by the schematic wavefunctions crossing the minimum energy path of the reaction. **b**, The ion signal measured at the MCP detector, after ToF separation. Shown is the average of 16 ToF traces, taken at the lowest H_2 density of 2.8×10^{14} cm^{-3} and 950 s interaction time. The inset is the signal multiplied by 30 to emphasize the H^- peak.

of 10 ms to 1 s are sufficient to observe the reaction kinetics. However, to study rate coefficients smaller than 10^{-18} cm^3 s^{-1}, densities beyond 10^{15} cm^{-3} and at the same time trapping times up to 1,000 s are required (Methods). Figure 1b shows the time-dependent appearance of a small peak of H^- ions after 950 s of trapping time at a density of 2.8×10^{14} cm^{-3}, which signifies that reaction (1) is actually taking place. Despite the high densities, no evidence for products from three-body recombination has been detected.

Figure 2 shows examples for measurements of the H^- fraction as a function of interaction time for different H_2 densities. We fit this fraction to the solution of rate equations (equations (4) and (5)), which include the growth of H^- and a background loss rate of H^- and D^-:

$$\frac{N_H(t)}{N_D(0)} = \left(\frac{k_H^{gr}}{k_H^{bg} - k_D^{bg} - k_H^{gr}}\right)\left(\left(e^{-(k_H^{gr}+k_D^{bg})t} - e^{-k_H^{bg}t}\right)\right) + \frac{N_H(0)}{N_D(0)}e^{-k_H^{bg}t}, \qquad (2)$$

where k_H^{gr} is the growth rate of H^-, k_X^{bg} denotes the respective background loss rates of H^- and D^- out of the trap, t is time, and $N_H(0)$ and $N_D(0)$ are the initial amounts of H^- and D^-. A separate fit to the decay of the D^- peak provides the sum of the D^- background loss rate and the H^- growth rate. The small amount of initial H^- comes from the trap loading: as high-energy D^- collides with the H_2 buffer gas during initial cooling, some H^- is created by means of classical over-the-barrier reactions.

The H^- growth rates that are extracted from the fits are plotted as a function of H_2 density in Fig. 3a; the background loss rates are shown in Fig. 3b. At the three lowest densities, the growth rates are consistent with a fit to linear dependence $k_H^{gr} = k_r n$ with $k_r = (5.2 \pm 1.6) \times 10^{-20}$ cm^3 s^{-1} (black dashed line in Fig. 3a). This rate coefficient corresponds roughly to one reaction occurring for every 10^{11} collisions, when the rate of all collisions that overcome the centrifugal barrier is described by the Langevin capture rate coefficient, which is about 2×10^{-9} cm^3 s^{-1}. This is, to our knowledge, the lowest measured bimolecular ion–molecule reaction rate constant by four orders of magnitude; see, for example, the Kinetic Database for Astrochemistry[28]. The rate coefficient agrees very well with the quantum theoretical prediction for the tunnelling rate coefficient for normal H_2 colliding with a thermal D^- velocity distribution[5] at a temperature of 15 K, which is indicated by the violet line in Fig. 3a. The width of the line represents the finite uncertainty of the ion temperature. A previous semiclassical statistical calculation based on an earlier potential energy surface provided a tunnelling rate coefficient that was about three orders of magnitude lower, which shows the enormous sensitivity of tunnelling rates to the theoretical methods[29].

At higher densities a strong deviation of the reaction rate from linear behaviour appears, accompanied by an increase in the trap loss rate of H^-, as seen in Fig. 3b. Such a non-linear behaviour has not been reported before for ion–molecule kinetics in traps, to our knowledge. To understand this phenomenon, one must take a closer look at the velocity distributions in RF ion traps. Using the adiabatic approximation, the ion velocity can be separated into micromotion, which is caused by the RF voltages and gives rise to the effective trapping potential, and secular motion, describing classical trajectories within the effective potential[25,26]. If an ion undergoes a collision during micromotion, energy can be transferred from the RF fields, increasing the amplitude of the secular motion. This is known as collisionally induced RF heating and has plagued ion traps since their invention. Owing to this RF heating, the velocity distribution is no longer described well by Maxwell–Boltzmann statistics, but brings about a high-energy tail in the ion distribution[27]. This must, in general, be considered for kinetics measurements, as a small number of reactions from the high-energy tail could skew the average measured reaction rates.

Following the non-extensive generalization of entropy by Tsallis[30], the velocity distribution in one dimension $f(v_i)$ of a trapped ion of mass m subjected to RF heating can be described by a q-exponential Tsallis distribution:

$$f(v_i) \propto \left(1 + (q-1)\frac{mv_i^2}{2k_BT}\right)^{\frac{1}{1-q}} \qquad (3)$$

which, in addition to the Boltzmann constant k_B and the temperature T, contains the parameter q that describes the strength of a power-law tail and can be generalized to the full velocity distribution (see equations (6)–(9) in the Methods). The limit $q \to 1$ recovers the Gaussian probability curve of a Maxwellian gas. For collision dynamics, the distribution of relative velocities between ions and neutrals is the relevant quantity.

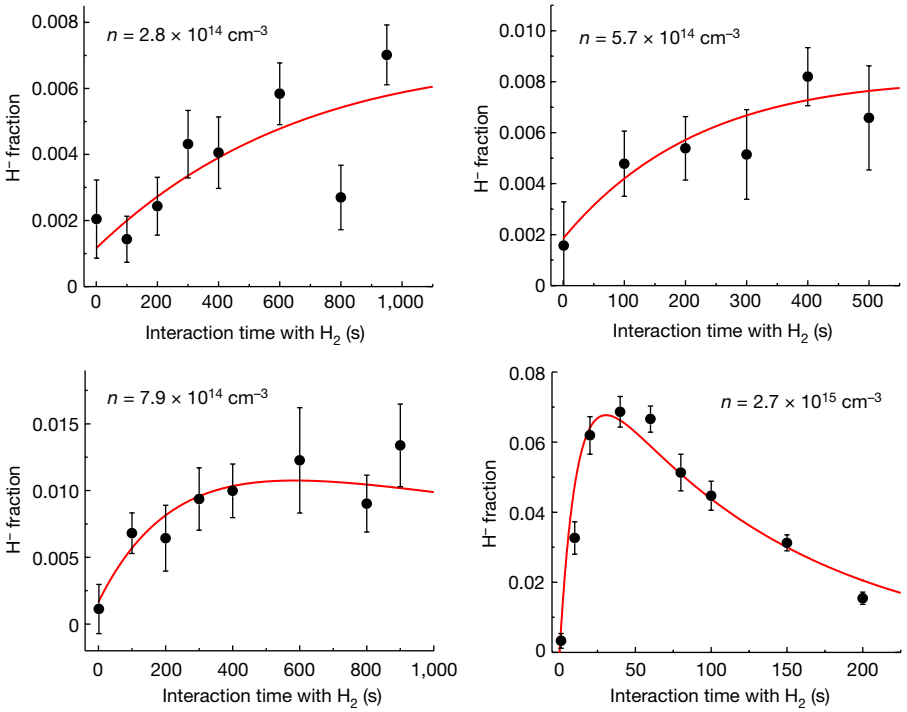

Fig. 2 | Ion–molecule reaction kinetics. The fractional amount of H^- present in the trap as a function of time is shown at four different densities. Red lines are fits to equation (2); error bars denote the standard error of the mean over 23, 8, 6 and 7 loops, respectively. As density increases, the loss of H^- out of the trap becomes prominent.

We obtain these by simulating the relative velocities between the Tsallis distribution of the ions and the Maxwell–Boltzmann distribution of the buffer gas.

The simulated relative velocity distributions are plotted in Fig. 3c for two different hydrogen densities and fitted with Tsallis distribution functions. The high-energy tail is notably increased at the high density, a phenomenon not observed in multipole ion traps before. This can be qualitatively understood to stem from a small mean free path of the trapped ions in the dense buffer gas. In multipole ion traps, RF heating occurs close to the turning points, where the micromotion

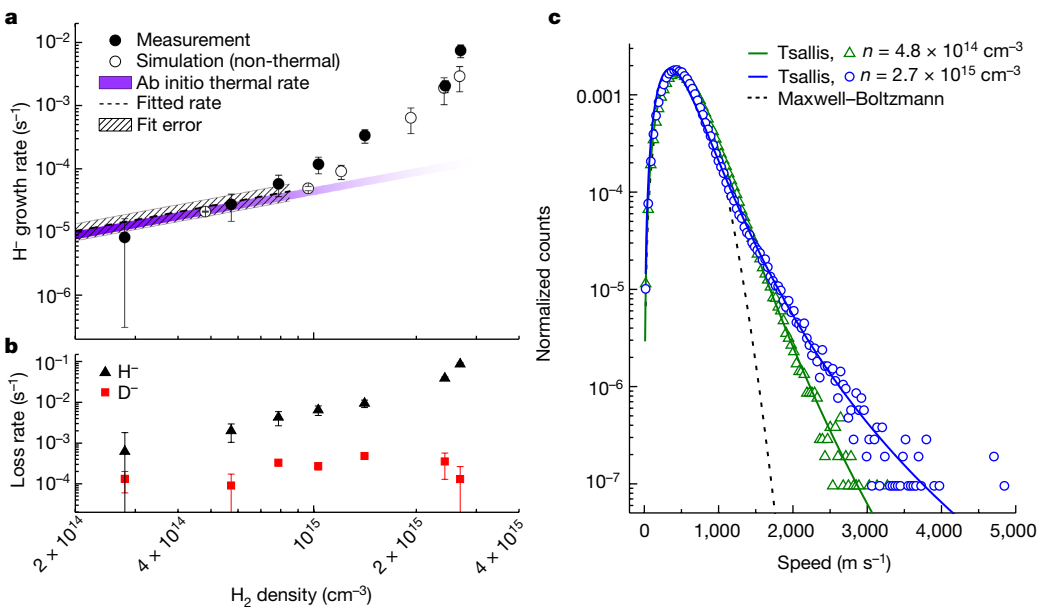

Fig. 3 | Density dependence of rates and velocity distributions. a, Black points show measurements of the H^- growth rate, with uncertainties given by the fits as in Fig. 2. The violet line is the theoretical prediction for the tunnelling rate for normal H_2 at the estimated collision temperature of 15 ± 5 K. The open circles show the result of a numerical simulation with error bars given by the standard deviation of 12 simulation runs. The black dashed line shows the linear fit to the measured rates at the lower densities. **b**, Loss rates of the parent and product ions out of the trap, with uncertainties as for the growth rate measurements. Elevated loss rates are seen above 7×10^{14} cm^{-3} of H_2, at which point the H^- growth rate begins to deviate from linear. **c**, The distribution of relative velocities between the ions and the Maxwell–Boltzmann hydrogen gas at 10 K for two different buffer gas densities. The distributions are fitted with a tail-weighted Tsallis function (equation (3)). A Maxwell–Boltzmann fit is shown for reference.

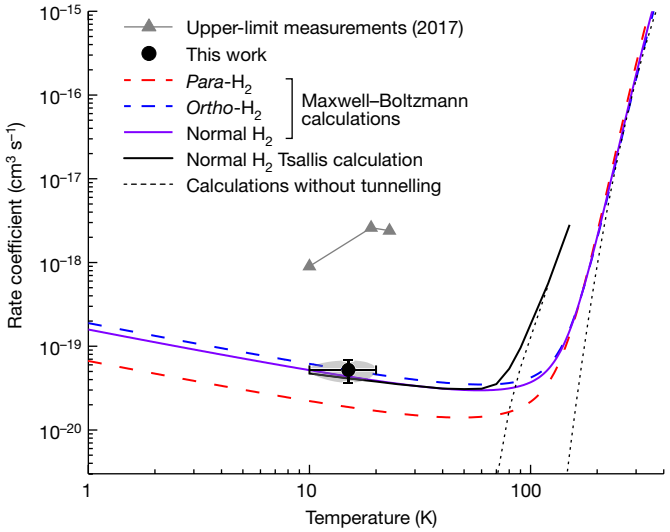

Fig. 4 | Tunnelling rate coefficient in comparison with theory. Measured and calculated reaction rate coefficients as a function of collision temperature. The black point with the error ellipse is the measurement presented in this work. The horizontal error is an estimate for our ion trap and the vertical error stems from the fit in Fig. 3a. Red and blue long-dashed lines show the Maxwell–Boltzmann averages of the calculation[5] for *ortho*-H_2 and *para*-H_2, with the violet solid line as the weighted average representing normal H_2. The solid black line shows the simulated result including the high-energy tail of the ion velocity distribution. The short-dashed black lines indicate the theoretical expectations (with and without high-energy tail) when tunnelling is excluded. The grey triangles show the upper-limit measurement[24] of 2017.

amplitude is large. At standard buffer gas densities, ions make multiple round trips through the trap between buffer gas collisions. Thus the probability for a subsequent collision to cool rather than heat is high. Then the ion velocity distribution has suppressed high-energy tails and is density independent. However, at densities above 10^{15} cm^{-3}, the mean free path becomes smaller than the trap diameter and comparable to the distances over which RF heating occurs (Extended Data Fig. 1). This can reduce the ion temperature in the trap centre, but causes a 'runaway' heating of the ions near the trap edges, which manifests itself as increased high-energy tails.

To determine the influence of the increased energy tails on the D^- reaction rate, we integrate the density-dependent Tsallis distributions for the relative velocity over the theoretical reaction probability (see Fig. 6 of Yuen et al.[5]) (see Methods section for details). The resulting reaction rate is plotted as open circles in Fig. 3a; the error bars represent the standard deviation of several simulations. This simulation shows an enhanced rate at high densities, which is in good agreement with the non-linear increase of the measured rate. Only the magnitude of the rate increase is slightly lower than that of the measurements. We expect that this extra heating is caused by differences between the real and simulated electric fields as a result of trap imperfections and patch potentials (Extended Data Fig. 2).

In the low-density limit, runaway heating is not present. The rate measurements for the lowest three densities in Fig. 3a agree well with a linear density dependence, and the H^- loss rates remain fairly constant here. Thus the reaction rate coefficient can be determined from the slope of these data points, as stated previously and plotted in Fig. 4. The theoretical tunnelling rate coefficient of Yuen et al.[5] is also shown in Fig. 4. The blue and red long-dashed lines show the theory for *ortho*-H_2 and *para*-H_2, respectively, with the violet solid line being the weighted average and representing the normal H_2 that was used in this experiment. This shows again that the measured rate coefficient agrees very well with the theoretical rate for normal H_2. In this temperature range, the rate coefficient is dominated by tunnelling. This becomes particularly clear from the short-dashed lines in Fig. 4, which show the theoretical rate coefficient when only over-the-barrier reactions without tunnelling are considered.

In this work we have measured the reaction rate constant of the proton exchange reaction D^- with H_2, which occurs by quantum mechanical tunnelling through the reaction barrier. The extremely small measured value of $(5.2 \pm 1.6) \times 10^{-20}$ cm^3 s^{-1} is in very good agreement with ab initio quantum scattering calculations. High-energy tails were found to influence the kinetics at high densities and at temperatures at which over-the-barrier reactions become active. This is an effect that will have to be included in other ion trap reaction measurements as well, in particular for endothermic or barrier-limited reactions. From our simulations, we know that these high-energy tails play only a minor role at the lower densities at which tunnelling takes place. This work shows how not only spectroscopic investigations, but also reaction kinetics can benchmark accurate quantum theoretical calculations. As such this broadens the understanding of tunnelling processes and will open up further research on the quantum dynamics of neutral and ionic reactions, for example, on the role of scattering resonances.

Online content

Any methods, additional references, Nature Portfolio reporting summaries, source data, extended data, supplementary information, acknowledgements, peer review information; details of author contributions and competing interests; and statements of data and code availability are available at https://doi.org/10.1038/s41586-023-05727-z.

1. McMahon, R. J. Chemical reactions involving quantum tunneling. *Science* **299**, 833–834 (2003).
2. Shannon, R. J., Blitz, M. A., Goddard, A. & Heard, D. E. Accelerated chemistry in the reaction between the hydroxyl radical and methanol at interstellar temperatures facilitated by tunnelling. *Nat. Chem.* **5**, 745–749 (2013).
3. Tizniti, M. et al. The rate of the F + H_2 reaction at very low temperatures. *Nat. Chem.* **6**, 141 (2014).
4. Yang, T. et al. Enhanced reactivity of fluorine with *para*-hydrogen in cold interstellar clouds by resonance-induced quantum tunnelling. *Nat. Chem.* **11**, 744–749 (2019).
5. Yuen, C. H. et al. Quantum-tunneling isotope-exchange reaction $H_2 + D^- \rightarrow HD + H^-$. *Phys. Rev. A* **97**, 022705 (2018).
6. Ferrière, K. M. The interstellar environment of our galaxy. *Rev. Mod. Phys.* **73**, 1031–1066 (2001).
7. Gerlich, D., Herbst, E. & Roueff, E. H_3^++HD→H_2D^++H2: low-temperature laboratory measurements and interstellar implications. *Planet. Space Sci.* **50**, 1275 (2002).
8. Tielens, A. G. G. M. The molecular universe. *Rev. Mod. Phys.* **85**, 1021 (2013).
9. Kitsopoulos, T. N., Buntine, M. A., Baldwin, D. P., Zare, R. N. & Chandler, D. W. Reaction product imaging: the H+D_2 reaction. *Science* **260**, 1605 (1993).
10. Harich, S. A. et al. Forward scattering due to slow-down of the intermediate in the H+HD→D+H_2 reaction. *Nature* **419**, 281 (2002).
11. Stevenson, D. & Hirschfelder, J. The structure of H_3, H_3^*, and of H_3^+. iv. *J. Chem. Phys.* **5**, 933–940 (1937).
12. Stärck, J. & Meyer, W. Ab initio potential energy surface for the collisional system H^-+H_2 and properties of its van der Waals complex. *Chem. Phys.* **176**, 83–95 (1993).
13. Wang, W. et al. Observations of H_3^- and H_3^- from dielectric barrier discharge plasmas. *Chem. Phys. Lett.* **377**, 512–518 (2003).
14. Ayouz, M., Lopes, R., Raoult, M., Dulieu, O. & Kokoouline, V. Formation of H_3^- by radiative association of H_2 and H^- in the interstellar medium. *Phys. Rev. A* **83**, 052712 (2011).
15. Zimmer, M. & Linder, F. Crossed-beam study of the H^-+D_2→HD(v′)+D^- rearrangement reaction in the collision energy range 0.3–3 eV. *J. Phys. B* **28**, 2671 (1995).
16. Belyaev, A. K., Colbert, D. T., Groenenboom, G. C. & Miller, W. H. State-to-state reaction probabilities for H^-+H_2, D_2 collisions. *Chem. Phys. Lett.* **209**, 309–314 (1993).
17. Haufler, E., Schlemmer, S. & Gerlich, D. Absolute integral and differential cross sections for the reactive scattering of H^-+D_2 and D^-+H_2. *J. Phys. Chem. A* **101**, 6441–6447 (1997).
18. Giri, K. & Sathyamurthy, N. Influence of reagent rotation on (H^-, D_2) and (D^-, H_2) collisions: a quantum mechanical study. *J. Phys. Chem. A* **110**, 13843–13849 (2006).
19. Zhang, W., Liu, Y. & He, X. Effect of reagent rotation on the integral cross-sections and isotopic branching of the reactions H^-+HD and D^-+HD. *Chem. Phys. Lett.* **489**, 237–241 (2010).
20. Wang, D. & Jaquet, R. Reactive scattering for different isotopologues of the H_3^- system: comparison of different potential energy surfaces. *J. Phys. Chem. A* **117**, 7492–7501 (2013).
21. Mikosch, J. et al. Inverse temperature dependent lifetimes of transient S_N2 ion–dipole complexes. *J. Phys. Chem. A* **112**, 10448–10452 (2008).
22. Herbst, E. et al. Calculations on the rate of the ion–molecule reaction between NH_3^+ and H_2. *J. Chem. Phys.* **94**, 7842–7849 (1991).
23. Markus, C. R. et al. Vibrational excitation hindering an ion–molecule reaction: the c-$C_3H_2^+$ – H2 collision complex. *Phys. Rev. Lett.* **124**, 233401 (2020).

24. Endres, E. S., Lakhmanskaya, O., Simpson, M., Spieler, S. & Wester, R. Upper limit of a tunneling reaction rate for $D^-+H_2 \rightarrow HD+H^-$. *Phys. Rev. A* **95**, 022706 (2017).
25. Gerlich, D. Ion-neutral collisions in a 22-pole trap at very low energies. *Phys. Scr.* **T59**, 256 (1995).
26. Wester, R. Radiofrequency multipole traps: tools for spectroscopy and dynamics of cold molecular ions. *J. Phys. B* **42**, 154001 (2009).
27. Asvany, O. & Schlemmer, S. Numerical simulations of kinetic ion temperature in a cryogenic linear multipole trap. *Int. J. Mass spectrom.* **279**, 147 (2009).
28. Wakelam, V. et al. A KInetic Database for Astrochemistry (KIDA). *Astrophys. J. Suppl. Ser.* **199**, 21 (2012).
29. Luo, H., Wu, Y. & Ju, L. Variational transition-state theory study of the $D^-+H_2 \rightarrow HD+H^-$ reaction and the $H^-+D_2 \rightarrow HD+D^-$ reaction. *Comput. Theor. Chem.* **963**, 475–478 (2011).
30. Tsallis, C. Possible generalization of Boltzmann–Gibbs statistics. *J. Stat. Phys.* **52**, 479–487 (1988).

Methods

Experiment

For the ion–molecule reaction experiments, we used a 22-pole linear RF trap configuration, which is described in detail elsewhere[25,26,31,32]. We created D^- and a small amount of H^- in a plasma discharge of deuterium gas. A Wiley–McLaren spectrometer accelerated the ions towards the trapping region, and we selectively loaded D^- into the multipole trap by ToF mass separation. Within the trap, the ions collided with normal-H_2 buffer gas (75% *ortho*-H_2 and 25% *para*-H_2) that had thermalized with the trap's copper housing at 10 K. At such low temperatures, measurements of average ion temperatures repeatedly showed temperatures warmer than the buffer gas[32,33] as a result of RF heating. Based on this, we estimated the collision temperature for the collisions of D^- with H_2 to be 15 ± 5 K. Both the imperfect ToF separation and collisions of D^- with H_2 during the initial cooling contributed to some initial H^- in the trap. Using helium as a buffer gas would have avoided the latter, but we have found the mass difference between He and D^- to have an adverse effect on trap lifetimes.

To be sensitive to low reaction rates, one desires high densities and long interaction times. Very high reactant gas densities can cause discharges at the high voltage of the microchannel plate (MCP) detector. To avoid this the MCP voltage was turned off before reactant gas was added. After the interaction time, the gas flow was switched off and the chamber pumped down until the pressure at the MCP detector was below 10^{-6} mbar. To probe long interaction times, extra effort was made to keep the vacuum chamber free of stray reactants such as water molecules, which limited experiments in the past[24]. In the measurements presented here, background lifetimes of D^- were in the order of three hours.

Pressures of H_2 were measured with a capacitive gauge connected to the trap housing by means of a Teflon tube. The capacitive gauge allows for an absolute pressure measurement independent of gas species. When calculating the gas densities in the trap, corrections for the temperature difference between the trap and the gauge, and for thermal transpiration effects, were performed[24]. The effects of thermal transpiration in the pressure regime in which we operated are pressure corrections ranging from 25% to 60%. Based on these, we estimated a 10% error in absolute density.

During extraction from the trap, we pulsed a small gate voltage to deflectors situated close to the trap opening to allow only a small fraction of the ion cloud with similar starting positions to pass undisturbed, producing a spatially localized ion packet. This substantially increased the ToF mass resolution and produced well-resolved ion peaks. However, the masses had begun to separate by the time they reached the deflectors, and so we probed slightly shifted parts of the ion packets of the two masses. We estimated an uncertainty of 20% in our measurements due to this effect.

To fit the H^- creation curves, we solved the set of equations given by:

$$\frac{\mathrm{d}}{\mathrm{d}t}N_{\mathrm{H}}(t) = k_{\mathrm{H}}^{\mathrm{gr}}N_{\mathrm{D}}(t) - k_{\mathrm{H}}^{\mathrm{bg}}N_{\mathrm{H}}(t) \tag{4}$$

$$\frac{\mathrm{d}}{\mathrm{d}t}N_{\mathrm{D}}(t) = -k_{\mathrm{H}}^{\mathrm{gr}}N_{\mathrm{D}}(t) - k_{\mathrm{D}}^{\mathrm{bg}}N_{\mathrm{D}}(t), \tag{5}$$

where N_{X} denotes the respective amounts of H^- and D^-, $k_{\mathrm{X}}^{\mathrm{bg}}$ denotes their respective background loss rates out of the trap and $k_{\mathrm{H}}^{\mathrm{gr}}$ is the growth rate of H^-. The solution is given by equation (2) in the main text. To achieve a more stable fit, a second-order Taylor expansion of the solution was used to fit the data at the two lowest densities.

Ion trajectory simulations and Tsallis distributions

An ion in an RF trap immersed in a cold buffer gas has been found to develop a power-law tail in the velocity distribution[27]. It can be modelled using a non-extensive generalization of entropy proposed by Tsallis[30] and developed further for a variety of physical systems[34–36].

To model the ion distribution, we performed molecular dynamics simulations; we calculated the ion trajectories by solving Newton's equation of motion numerically, and treated the collisions as those in a hard-sphere collision model using a Monte Carlo approach. We used an ideal time-varying multipole field in the radial direction and a quadrupole plus octupole static field in the axial direction, along with random collisions with a background buffer gas. Ion–ion interactions were neglected because of the low ion density within the trap. As collision frequency increased, the bulk of the ions moved closer to the trap centre. Simultaneously, the number of ions at the outer edges increased (Extended Data Fig. 1a). The energies of the outer ions also increased with higher collision frequency (Extended Data Fig. 1b). This indicates a runaway heating effect due to multiple sequential heating collisions, which becomes pronounced when the mean free path of the ions becomes small compared with the mean distance travelled up the trap potential.

We fitted each dimension of the velocity distribution of the ions $f_{1\mathrm{D}}(v_i)$ (see also equation (2)), with $i = x, y, z$, to the q-exponential

$$f_{1\mathrm{D}}(v_i) = N_{1\mathrm{D}}\left(1 + (q-1)\frac{mv_i^2}{2k_{\mathrm{B}}T}\right)^{\frac{1}{1-q}}, \tag{6}$$

where m is the ion mass, T is the temperature and q is the parameter giving the strength of the tail, with normalization factor:

$$N_{1\mathrm{D}} = \left(\frac{m}{2k_{\mathrm{B}}T}\right)^{1/2}\frac{\Gamma\left(\frac{1}{q-1}\right)}{\Gamma\left(\frac{3-q}{2(q-1)}\right)}\left(\frac{q-1}{\pi}\right)^{1/2} \tag{7}$$

for $1 < q < 3$. The two radial directions exhibit the same distribution as a result of symmetry. From the one-dimensional velocity distribution, one can derive the full distribution of speeds v:

$$f_{3\mathrm{D}}(v) = N_{3\mathrm{D}}4\pi v^2\left(1 + (q-1)\frac{mv^2}{2k_{\mathrm{B}}T}\right)^{\frac{1}{1-q}} \tag{8}$$

with normalization factor:

$$N_{3\mathrm{D}} = \left(\frac{m}{2k_{\mathrm{B}}T}\right)^{3/2}\frac{\Gamma\left(\frac{1}{q-1}\right)}{\Gamma\left(\frac{1}{q-1}-\frac{3}{2}\right)}\left(\frac{q-1}{\pi}\right)^{3/2}. \tag{9}$$

Equation (8) does not exactly describe the distribution of relative velocities between a Tsallis and a Maxwell–Boltzmann distribution, but it can be used empirically as a reasonable-fit function (Fig. 3c). Because the effects of the high-energy tail were of prime interest in this work, we fitted the logarithm of the distribution function (equation (8)) to the logarithm of the distribution, which puts more weight on the high-energy tail.

The calculations for the reaction rate coefficients without tunnelling, shown in Fig. 4, were performed using a step function as the energy barrier. The reaction rates come from the percentage of ions that have a collision energy above this barrier. The height of the barrier was adjusted such that the rate without tunnelling matches the calculated rate from the Maxwell–Boltzmann distribution at high temperatures from Yuen et al.[5]. The corresponding barrier height is 275 meV, which is consistent with the experimentally measured barrier[17] of 330 ± 60 meV.

Data availability

The datasets used for this study are available on zenodo.org at https://doi.org/10.5281/zenodo.7148592. Source data are provided with this paper.

Code availability

The code used during this study is available from the corresponding author on reasonable request.

31. Best, T. et al. Absolute photodetachment cross-section measurements for hydrocarbon chain anions. *Astrophys. J.* **742**, 63 (2011).
32. Endres, E. S. et al. Incomplete rotational cooling in a 22-pole ion trap. *J. Mol. Spectrosc.* **332**, 134 (2017).
33. Jusko, P., Asvany, O., Wallerstein, A.-C., Brünken, S. & Schlemmer, S. Two-photon rotational action spectroscopy of cold OH^- at 1 ppb accuracy. *Phys. Rev. Lett.* **112**, 253005 (2014).
34. Silva, R. Jr, Plastino, A. R. & Lima, J. A. S. A Maxwellian path to the *q*-nonextensive velocity distribution function. *Phys. Lett. A* **249**, 401–408 (1998).
35. Jiulin, D. The nonextensive parameter and Tsallis distribution for self-gravitating systems. *Europhys. Lett.* **67**, 893–899 (2004).
36. Rouse, I. & Willitsch, S. Superstatistical energy distributions of an ion in an ultracold buffer gas. *Phys. Rev. Lett.* **118**, 143401 (2017).

Acknowledgements We thank V. Kokoouline, C. H. Yuen and M. Ayouz for fruitful discussions. This work has been supported by the Austrian Science Fund (FWF) through Project I2920-N27 and through the Doctoral Programme Atoms, Light, and Molecules, Project No. W1259-N27.

Author contributions R. Wester conceived the experiment and supervised the project. R. Wild, M.N., M.S. and T.D.T. carried out the measurements. R. Wild, with support from M.N. and R. Wester, carried out the simulations. R. Wild and R. Wester wrote the manuscript, which was discussed and approved by all authors.

Competing interests The authors declare no competing interests.

Additional information

Supplementary information The online version contains supplementary material available at https://doi.org/10.1038/s41586-023-05727-z.

Correspondence and requests for materials should be addressed to Roland Wester.

Peer review information *Nature* thanks the anonymous reviewers for their contribution to the peer review of this work.

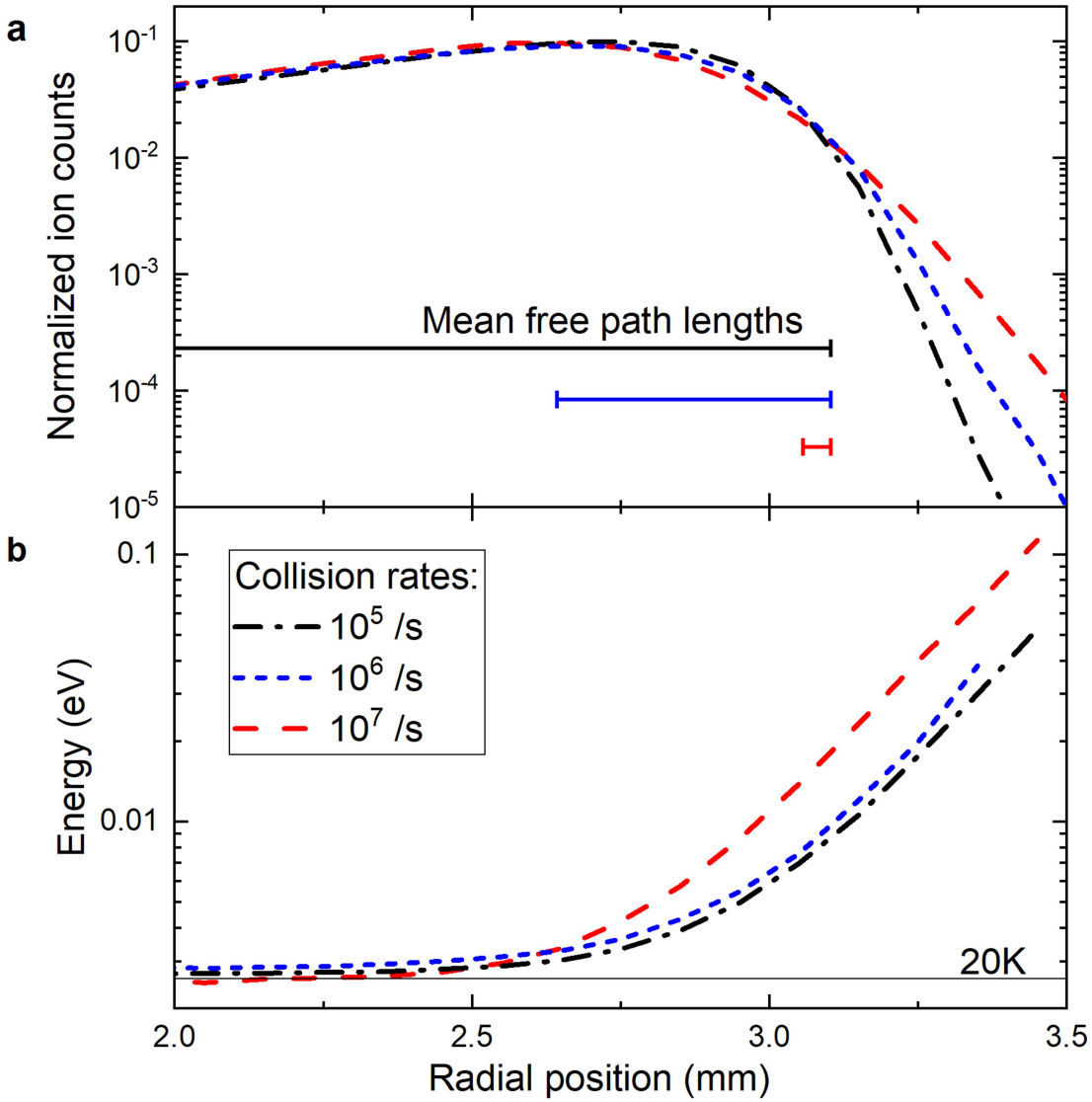

Extended Data Fig. 1 | Ion trap simulations for different densities. Distributions of ion number and energy as a function of the radial position in the trap, at different collision rates and with a buffer gas temperature of 20 K. **a** With higher collision rates, ions move, on average, slightly closer to the centre, but also increase in number at large radii. Mean free path lengths are shown for reference. **b** When the mean free path becomes small, energies close to the trap rods increase substantially, indicating multiple heating collisions before moving away from the trap edges. The collision rates correspond to H_2 densities of 4.8×10^{13}, 10^{14} and 10^{15} cm^{-3}, respectively.

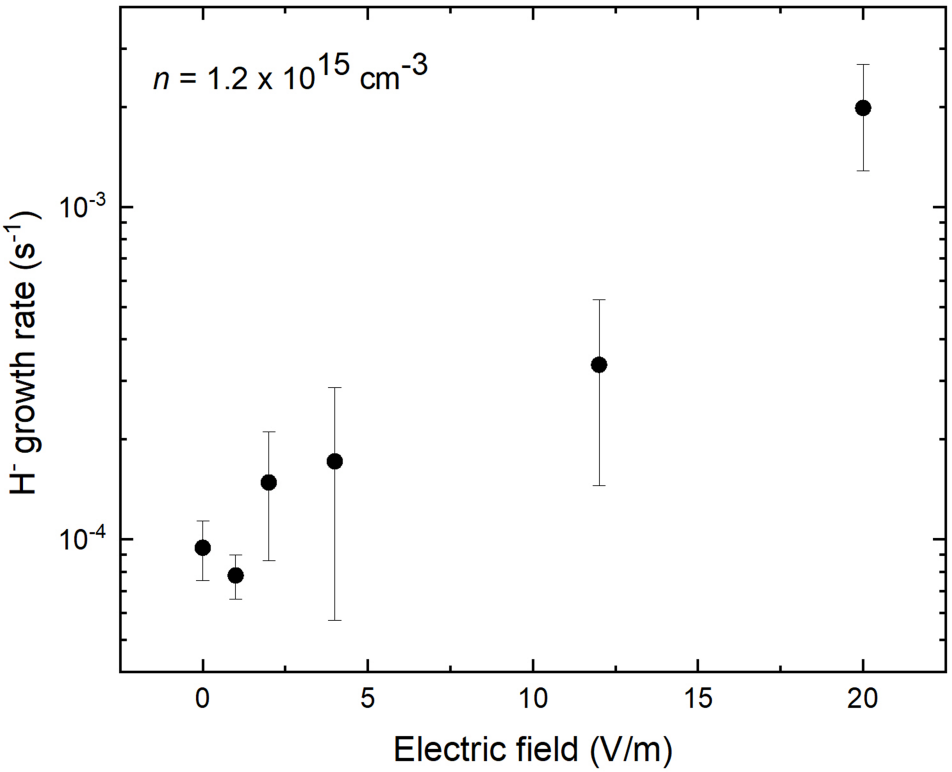

Extended Data Fig. 2 | Ion trap simulations including stray electric fields. Numerical simulations of the expected reaction rates at a hydrogen gas density of 1.2×10^{15} cm^{-3}, with error bars as in Fig. 3a. The electric fields were chosen to be homogeneous and oriented in one direction perpendicular to the RF trapping rods, which has the effect of slightly pushing the ions towards the RF electrodes on one side. The simulations show that an extra field on the order of 10 mV mm^{-1} could account for the higher measured reaction rates at this density.